ISSN 1063-7745, Crystallography Reports, 2024, Vol. 69, No. 7, pp. 1–7. © Pleiades Publishing, Inc., 2024.

NANOMATERIALS AND CERAMICS

Investigation of the Parameters of the Zinc Oxide Band Structure under High-Energy Mechanical Grinding

I. A. Filippov[a], A. A. Karmanov[a,*], N. D. Yakushova[a], E. I. Gurin[a], A. C. Komolov[b], and I. A. Pronin[a]

[a] *Penza State University, Penza, 440026 Russia*

[b] *St.Petersburg University, St Petersburg, 199034 Russia*

**e-mail: starosta07km1@mail.ru*

Received June 19, 2024; revised July 5, 2024; accepted July 7, 2024

Abstract—A controlled modification of the parameters of the zinc oxide band structure has been demonstrated using the methods and approaches of nanostructure engineering by varying the duration of high-energy mechanical grinding. It has been shown that an increase in the dispersion time increases the monodispersity of ultrafine ZnO powder particles. A decrease in the zinc oxide band gap with increasing grinding duration is established based on spectrophotometric investigations. A nonmonotonic time dependence of the top of the valence band, as well as a high-energy shift of the valence and conduction bands for all dispersion durations, are demonstrated using experimental X-ray photoelectron spectroscopy data.

DOI: 10.1134/S106377452460162X

INTRODUCTION

The nanomaterials based on metal oxides, such as ZnO, SnO_2, TiO_2, etc., are a subject of intensive research due to their unique electrophysical, optical, and photocatalytic properties [1, 2], which, in turn, are determined by the parameters of their energy-band structure [3]. Particular attention is paid to the materials produced in the form of thin films, as well as powders with a controlled crystallite size [4, 5]. At the same time, it has been shown that the properties of metal oxide nanomaterials can be varied using macrolevel impacts (for example, by changing the film annealing temperature and duration) [6, 7], as well as by controlling the processes of material self-assembling and self-organization at the initial synthesis stages. For example, the self-assembling of metal oxide ZnO and SiO_2–SnO_2 micro- and nanostructures can be controlled by exposing the film-forming sol to hard UV irradiation or cooling it to liquid nitrogen temperatures [8, 9].

Zinc oxide stands out among the aforementioned metal oxides; this compound is an *n*-type wide bandgap semiconductor (the bandgap is ~3.3 eV); its conductivity type is associated with oxygen vacancies in the wurtzite crystal lattice and interstitial zinc [10]. ZnO can be synthesized by various physical and chemical methods, among which of particular importance are the sol–gel technology [11, 12], as a prominent representative of the bottom–top nanotechnological approach, and high-energy mechanical grinding, corresponding to the top–bottom nanotechnology [13, 14]. New methods and approaches of nanostructure engineering, related to the fabrication of zinc oxide micro- and nanostructures in combined sol–gel systems, were developed in [15]. The formation of surface morphology of ZnO films with many levels of spatial hierarchy was demonstrated [15].

In this study, we develop an alternative approach of nanostructure engineering of metal oxide nanomaterials, based on macrolevel treatments, namely, high-energy mechanical grinding. This approach is a relatively simple way to control the surface properties of a nanomaterial, in which the type and concentration of adsorption centers are often a nonmonotonic and even periodic function of the dispersion time. Based on this approach, one can obtain zinc oxide powders for numerous applications, including energy-efficient photocatalysts [16]; electrodes for ultracapacitors [17]; and various types of sensor devices, in particular, gas sensors [18, 19].

A topical problem is the variation in the parameters of the ZnO band structure in dependence of the crystal structure of the material and the morphology and size of the particles forming it. For example, there is still no full understanding of the mechanisms of changing the band gap and the position of the valence band top for nanostructured zinc oxide [20]. The purpose of this study was to develop methods and approaches of nanostructure engineering providing controlled modification of the parameters of the ZnO band structure under high-energy mechanical grinding. Achieving this goal is of interest for obtaining a complete pattern of the changes occurring in a wide-bandgap semiconductor metal oxides, both during

their formation due to the aggregation of single nanoelements, having, in particular, a fractal nature [21], and using macrolevel impacts.

EXPERIMENTAL

Synthesis of ultrafine zinc oxide powders. Commercial ZnO powder (AR Vekton) was subjected to high-energy mechanical grinding using an attritor (Union Process HD/01). To this end, a shaft with ZrO_2 cylindrical blades was placed in the attritor glass, and zirconium dioxide balls 3 mm in diameter (grinding bodies) were poured into it. Then wet grinding was carried out. To this end, after turning the attritor on (the stirring speed was 100 rpm), a commercial ZnO powder was poured in until it was uniformly distributed over the glass volume, and isopropyl alcohol (AR Vektron) was added. After closing the attritor lid, the shaft rotation speed was gradually increased to 500 rpm. Liquid samples with a mass of 40 g, characterized by dispersion times of 1, 3, and 5 h, were chosen using a doser and dried at 70°C for 24 h. Then the samples were cooled to room temperature and ground in an agate mortar to eliminate the agglomerates formed during drying [13].

Investigation of ultrafine zinc oxide powders by scanning electron microscopy. Photomicrographs of samples with different times of high-energy mechanical grinding were obtained on a Hitachi S3400N scanning tunneling microscope (Japan) in the secondary-electron mode. The photomicrographs were processed and analyzed using an ImageJ graphic editor. The geometrical sizes of particles were evaluated, after which a size distribution histogram was constructed based on the measurement results for a part of an ultrafine ZnO powder.

Spectrophotometric investigations of ultrafine zinc oxide powders. The diffuse reflection spectra for the samples with different times of high-energy mechanical grinding were recorded on a SF-56 spectrophotometer (OKB Spectr) using a diffuse reflection attachment PDO-6. The measurements were carried out in the spectral range of 350–600 nm; the discretization step was 1 nm.

Investigations of ultrafine zinc oxide powders by X-ray photoelectron spectroscopy (XPS). The XPS spectra were measured under ultrahigh vacuum conditions ($p \sim 10^{-7}$ Pa) on an Escalab 250Xi complex photoelectron spectrometer (Thermo Fisher Scientific Inc.) with the AlK_α photon energy equal to 1486 eV. To eliminate surface contaminations of powders due to atmospheric adsorbates, the samples were etched by Ar^+ ions ($I_i = 1$ μA, $t_i = 30$ s). The spectrometer energy scale was calibrated using an Au surface (cleaned by sputtering) as a reference, so that the binding energy of the Au4f7/2 peak was established at a level of 84.0 eV.

RESULTS AND DISCUSSION

Figure 1 presents the photomicrographs of the commercial ZnO powder and ultrafine powders on its base, obtained at different times of high-energy mechanical grinding, made with a scanning tunneling microscope (STM). An analysis of the images shows that the original zinc oxide powder consist mainly of elongated hexagonal prisms with a base 150–300 nm in size (Fig. 1); the powder particles are characterized by high dispersion, a consequence of which is the presence of large elements with sizes of 350 nm or more (see the inset in Fig. 1a and the corresponding size distribution histogram for ZnO particles). High-energy mechanical grinding not only decreases the average size of particles but also substantially increases their monodispersity (Figs. 1b–1d). Grinding for 5 h provides practically complete destruction of large elements in the powder composition into smaller ones, due to which the average particle size significantly decreases: to 150–200 nm (the histogram in the inset in Fig. 1d). According to the X-ray diffraction data, high-energy mechanical grinding also essentially diminishes the coherent scattering regions (from 37 ± 1 to 21 ± 1 nm) and increases microstrains (from ~0.3 to ~0.6%) [22]. This change in the particle sizes and surface morphology may cause a change of the band structure of the samples, mainly due to the formation of defects (including surface defects) and microstrains rather than due to size effects.

The bandgap optical width of studied samples with different times of high-energy mechanical grinding was determined using diffusion reflection spectra (Fig. 2). An analysis of these spectra shows that an increase in the dispersion time significantly decreases the diffuse reflection factor in the entire spectral range under consideration (350–600 nm), which corresponds to decreasing the average size of ZnO powder particles during grinding and agrees with the scanning electron microscopy data.

To estimate the optical width of the band gap (ΔE_g) of the studied ZnO powders, we used the Tauc construction [23]:

$$(\alpha h\nu)^n = A(h\nu - E_g),$$

where α, $h\nu$, A, and E_g are, respectively, the absorption coefficient, the photon energy, the fit parameter, and the bandgap optical width. The n values for direct and nondirect gap semiconductors are 2 and 0.5, respectively.

The relationship between the absorption coefficient and diffuse reflection factor is given by the Kubelka–Munk function:

$$\alpha \sim F(R) = \frac{(1-R)^2}{2R},$$

where R is the diffuse reflection factor.

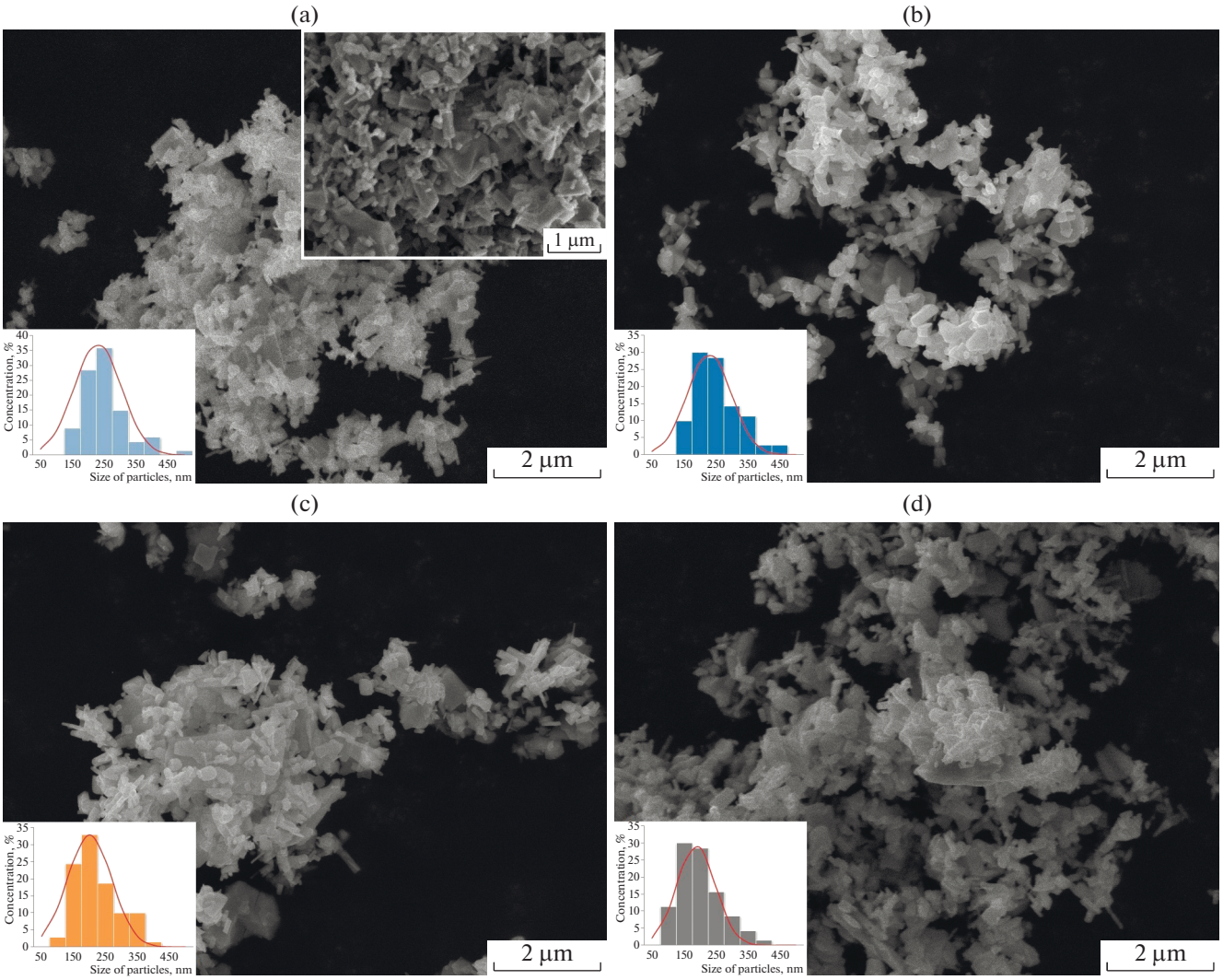

Fig. 1. SEM images of the surface of the (a) original ZnO powder and (b–d) powders with different times of high-energy mechanical grinding: (b) 1, (c) 3, and (d) 5 h.

Figure 3 presents the Tauc construction for the studied samples with different times of high-energy mechanical grinding, on the assumption that zinc oxide is a direct gap semiconductor [24]. For each graph, a linear section was selected, which was extrapolated to the intersection with the abscissa axis; at the same time, the point of intersection corresponds to the bandgap optical width.

An analysis of the curves presented in Fig. 3a shows that for the bandgap optical width for the commercial ZnO powder is 3.28 eV, whereas for the sample with a grinding time of 1 h it is $\Delta E_g \approx 3.27$ eV. Increasing the dispersion duration up to 3 and 5 h noticeably decreases the ΔE_g value: to ~3.25 and ~3.24 eV, respectively (Fig. 3b), which is apparently related to the microstrains of the zinc oxide crystal lattice and vacancies in the oxygen sublattice, leading to expansion of Urbach tails [25], and agrees with the X-ray diffraction data.

Further studies of the valence band of ZnO powders with different times of high-energy mechanical grinding and their relationship with the bandgap optical width were performed by XPS. Figure 4 presents the XP spectra of the valence band for the samples studied in comparison with the commercial zinc oxide powder. The position of the valence band top was determined by extrapolating the edge of the valence band spectrum with the lowest binding energy to the intersection with the abscissa axis [26, 27]. It was assumed that the Fermi level position corresponds to zero binding energy.

An analysis of the spectra shows that the valence band top has energy of 2.47 eV with respect to the Fermi level for the original powder (Fig. 4a); taking into account that the known bandgap is 3.28 eV, this

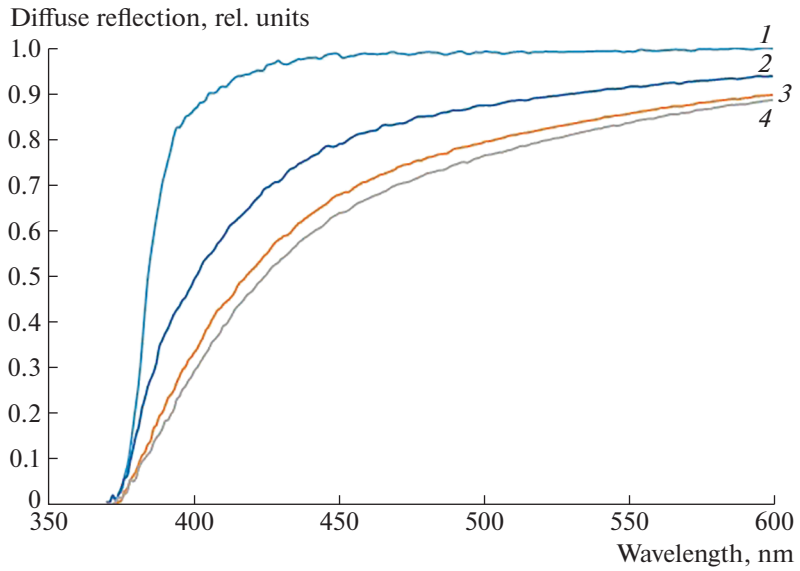

Fig. 2. Diffuse reflection spectra of the (*1*) original ZnO powder and (*2–4*) powders with different times of high-energy mechanical grinding: (*2*) 1, (*3*) 3, and (*4*) 5 h.

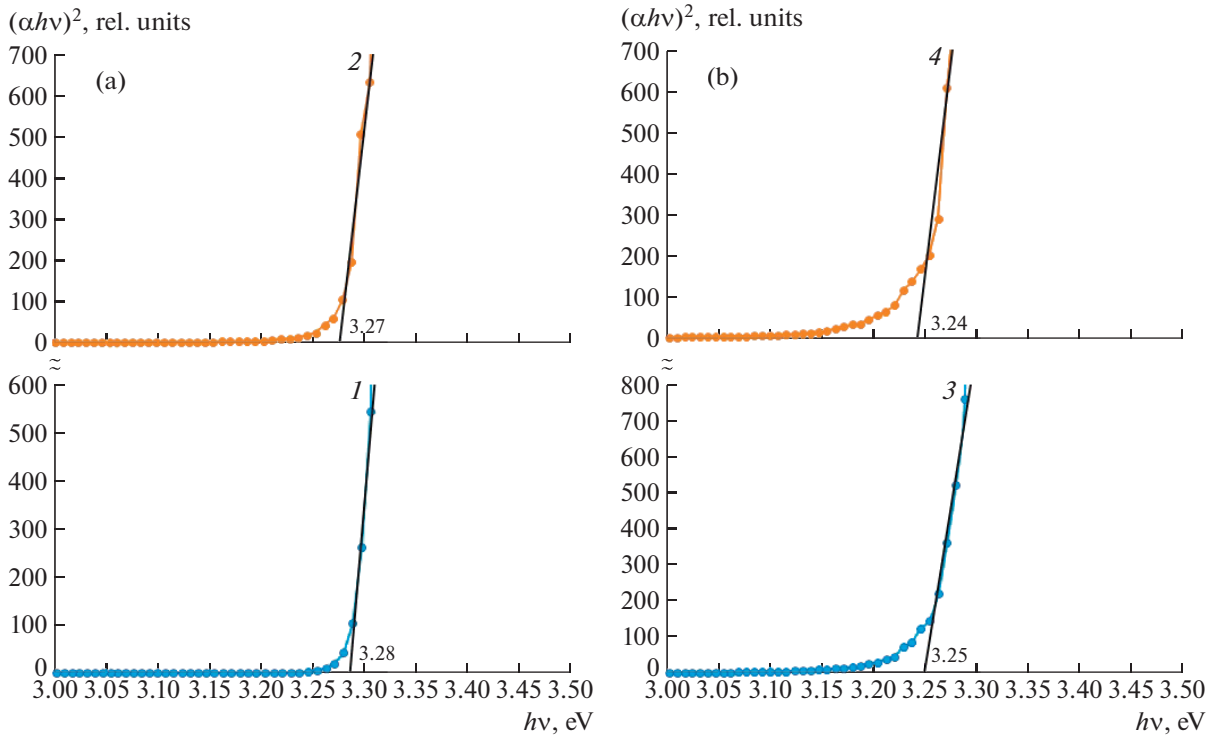

Fig. 3. The Tauc construction for determining the optical width of the band gap of the (*1*) original ZnO powder and (*2–4*) powders with different times of high-energy mechanical grinding: (*2*) 1, (*3*) 3, and (*4*) 5 h.

fact confirms the electronic type of the material conductivity. For the sample with a grinding time of 1 h, the valence band maximum has energy of ~1.87 eV, which is 0.6 eV smaller than that for the commercial ZnO powder, and corresponds to the valence band shift to higher energies. A similar shift is characteristic for the lower unoccupied orbital of the conduction band; i.e., a shift to high energies is observed for both the valence and conduction bands, a fact suggesting consistency of the Fermi level position [28] when

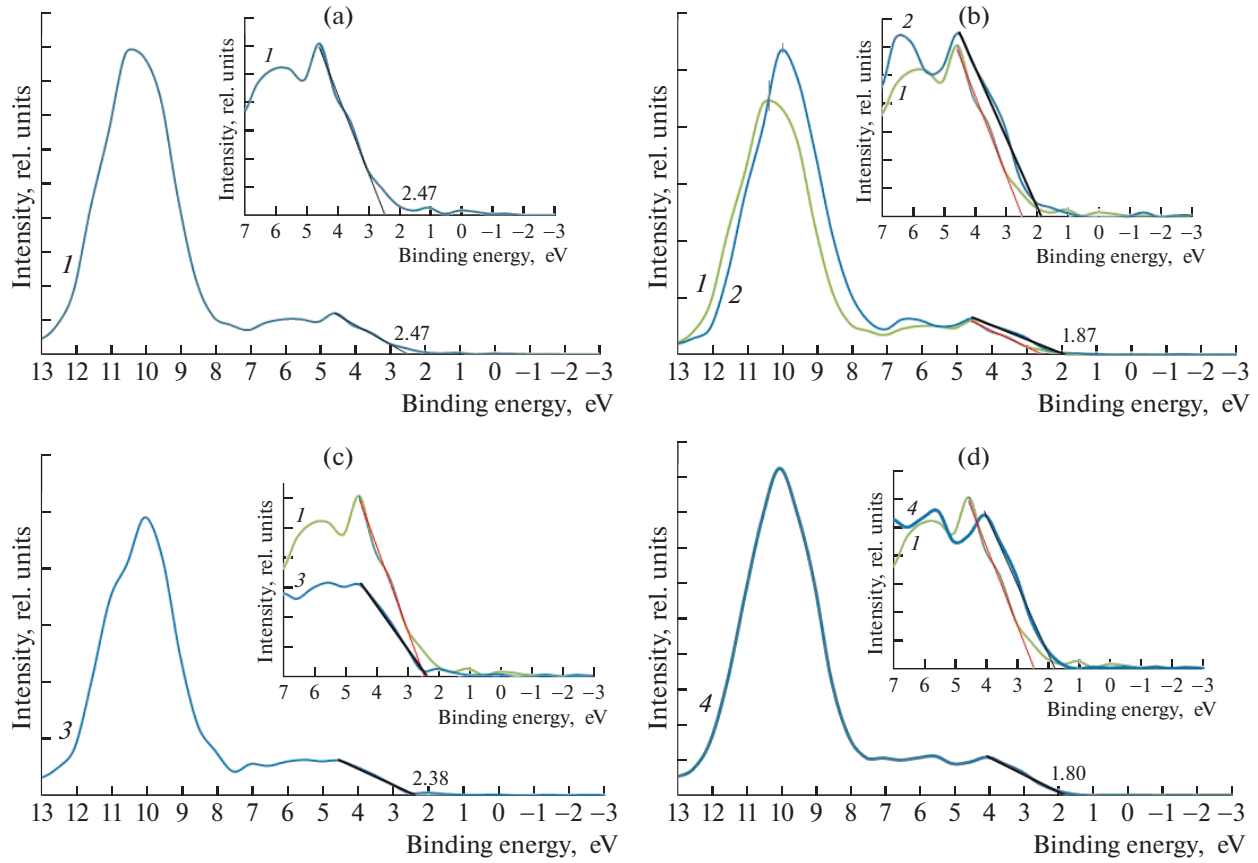

Fig. 4. XP spectra of the valence band of the (*1*) original ZnO powder and (*2–4*) powders with different times of high-energy mechanical grinding: (*2*) 1, (*3*) 3, and (*4*) 5 h.

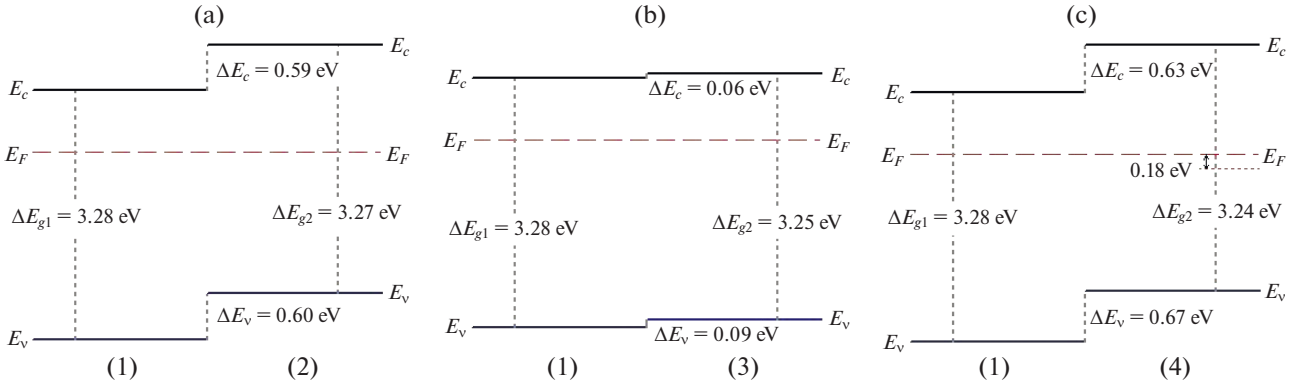

Fig. 5. Energy band diagrams of the (*1*) original ZnO powder and (*2–4*) powders with different times of high-energy mechanical grinding: (*2*) 1, (*3*) 3, and (*4*) 5 h.

comparing samples. The increase in the grinding time to 3 and 5 h leads to a nonmonotonic dependence of the position of the valence band top on the grinding time, which corresponds to characteristic energies of 2.38 and 1.80 eV, respectively.

Energy band diagrams of ZnO powders with different times of high-energy mechanical grinding are presented in Fig. 5; they generalize the results of spectrophotometric investigations of the bandgap optical width and XPS of the valence band.

An analysis of these diagrams shows that a shift of the valence band (ΔE_v) and the conduction band (ΔE_c) to high energies is characteristic for all grinding times. At the same time, the greatest shift is characteristic for ZnO powders with a dispersion time of 5 h (ΔE_v = 0.67 eV and ΔE_c = 0.63 eV), whereas the samples with

a grinding time of 3 h (ΔE_v = 0.09 eV and ΔE_c = 0.06 eV) exhibit the smallest shift. For all materials, the Fermi level lies above the middle of the band gap, at least by ~0.18 eV (Fig. 5c, curve *4*); based on this, one can conclude that they are *n*-type zinc oxides.

The nonmonotonicity of the time dependence of the band structure parameters for the samples has a complicated character, which is not completely clear; one of possible explanations is the presence of various defects in zinc oxide (including surface defects), whose character changes during high-energy mechanical grinding. This assumption correlates with the results of previous investigations of the evolution of acid-base properties of the surface of the ZnO powders obtained by grinding in attritor [29]. In particular, it was previously established that, after 1-h dispersion, the concentration of Louis-type oxide centers with pK_a = 14.2 (these centers are presented by surface zinc atoms, experiencing deficit of neighbors, in various configurations) is reduced; after 3-h grinding, it sharply increases; and, after 5-h grinding, it decreases to values close to the original ones. The time dependence of the concentration of Bronsted base centers with pK_a = 7.3–12.8, which has a pronounced maximum for the dispersion time of 3 h, behaves similarly. These centers correspond to surface Zn–OH hydroxyl groups in different configurations, and their amount correlates with the content of vacancies in the oxygen sublattice on the sample surface. The aforementioned features of the evolution of acid–base properties of unltrafine ZnO powders confirm the suggestion about the influence of various defects, including vacancies in the oxygen sublattice and zinc atoms with deficit of neighbors, on the band structure parameters. It should also be noted that a change of the band structure of the samples may be related to a chemical fixation of carbon dioxide in the carbonate-like form on their surface [30].

The analysis of the XP spectra of the valence band shows also a shift of the 3*d* orbital with a binding energy maximum of ~10.5 eV. This shift to lower binding energies (relative to the original powder) is observed for all grinded ZnO powders; it is ~0.5 eV by an order of magnitude (Fig. 4b). One of possible explanations of the observed feature of the XP spectra is a change in the electronic configuration of the transition metal ion Zn^{2+} [28, 31] as a result of the change in its position in the crystal lattice (caused, in particular, by microstrains and oxygen sublattice vacancies).

CONCLUSIONS

In the present work we developed methods and approaches of nanostructure engineering providing controlled modification of the band structure parameters of zinc oxide under high-energy mechanical grinding. It is shown that dispersion of ZnO powder is accompanied by both variation in the particle morphology (increasing monodispersity and decreasing the average size of elements to 100–150 nm) and a significant variation in the band structure parameters. Based on the spectrophotometric data, it was found that the bandgap of ZnO powders decreases by 0.04 eV relative to the commercial powder as a result of 5-h grinding. Using the XP spectra of the top of the valence band, we demonstrated a nonmonotonic character of its dependence on the grinding time. The analysis of the energy band diagrams of ultrafine zinc oxide powders showed a shift of the valence and conduction bands to higher energies for all investigated samples (0.09–0.67 eV for the valence band top and 0.06–0.63 eV for the lower unoccupied orbital of the conduction band). The obtained results may be of interest for developing methods of fabrication of metal oxide materials with specified structural parameters and features of the band structure for a wide range of practical applications.

ACKNOWLEDGMENTS

This work was performed using equipment of the Research Resource Center "Physical Methods of Surface Investigation" of the Research Park of Saint-Petersburg State University.

FUNDING

This study was supported by the Russian Science Foundation (grant no. 23-79-01280, https://rscf.ru/project/23-79-01280/).

CONFLICT OF INTEREST

The authors of this work declare that they have no conflicts of interest.

REFERENCES

1. Z. Chen, B. Zhou, M. Xiao, et al., Sci. Adv. **10** (2024). https://doi.org/10.1126/sciadv.adk6856
2. S. Rajan, A. Venugopal, H. Kozhikkalathil, et al., Mater. Today: Proc. (2023). https://doi.org/10.1016/j.matpr.2023.05.680
3. M. I. Khan, M. Irfan, M. Fatima, et al., Ceram. Int. **49**, 29622 (2023). https://doi.org/10.1016/j.ceramint.2023.06.188
4. J. Liu, J. Lv, H. Xiong, et al., J. Alloys Compd. **898**, 162875 (2022). https://doi.org/10.1016/j.jallcom.2021.162875
5. M. C. Uribe-López, M. C. Hidalgo-López, R. López-González, et al., J. Photochem. Photobiol. A **404**, 112866 (2021). https://doi.org/10.1016/j.jphotochem.2020.112866
6. H. Chenaina, C. Messaadi, J. Jalali, et al., Inorg. Chem. Commun. **124**, 108401 (2021). https://doi.org/10.1016/j.inoche.2020.108401

7. K. S. Lokesh, J. N. Kumar, V. Kannantha, et al., Mater. Today: Proc. **24**, 201 (2020). https://doi.org/10.1016/j.matpr.2020.04.268
8. S. E. Igoshina, E. A. Lykov, N. D. Yakushova, et al., Russ. Phys. J. **66**, 84 (2023). https://doi.org/10.17223/00213411/66/2/84
9. I. A. Pronin, I. A. Averin, N. D. Yakushova, et al., Arab. J. Sci. Eng. **42**, 4299 (2017). https://doi.org/10.1007/s13369-017-2804-8
10. N. A. Vorobyeva, M. N. Rumyantseva, P. A. Forsh, et al., Semiconductors **47**, 650 (2013). https://doi.org/10.1134/S1063782613050242
11. A. V. Meshcheryakov, A. P. Sigaev, I. A. Averin, et al., Nano Microsyst. Tech. **23**, 186 (2021). https://doi.org/10.17587/nmst.23.186-192
12. T. Amakali, L. S. Daniel, V. Uahengo, et al., Crystals **10**, 132 (2020). https://doi.org/10.3390/cryst10020132
13. I. A. Averin, I. A. Pronin, N. D. Yakushova, et al., Tech. Phys. **64**, 1330 (2019). https://doi.org/10.1134/S1063784219090020
14. A. Peleš, V. P. Pavlović, S. Filipović, et al., J. Alloys Compd. **648**, 971 (2015). https://doi.org/10.1016/j.jallcom.2015.06.247
15. A. A. Karmanov, I. V. Sukhov, N. D. Yakushova, et al., Nano Microsyst. Tech. **26**, 96 (2024). https://doi.org/10.17587/nmst.26.96-103
16. Y. Lin, H. Hu, and Y. H. Hu, Appl. Surf. Sci. **502**, 144202 (2020). https://doi.org/10.1016/j.apsusc.2019.144202
17. S. Najib, F. Bakan, N. Abdullayeva, et al., Nanoscale **12**, 16162 (2020). https://doi.org/10.1039/D0NR03921G
18. I. A. Averin, I. A. Pronin, A. A. Karmanov, et al., RF Patent No. RU 2718710 C1 (2019).
19. C. N. Wang, Y. L. Li, F. L. Gong, et al., Chem. Rec. **20**, 1553 (2020). https://doi.org/10.1002/tcr.202000088
20. S. A. Ansari, M. M. Khan, S. Kalathil, et al., Nanoscale **5**, 9238 (2013). https://doi.org/10.1039/C3NR02678G
21. I. A. Averin, I. A. Pronin, N. D. Yakushova, et al., Tech. Phys. **64**, 1821 (2019). https://doi.org/10.1134/S1063784219120028
22. I. A. Pronin, I. A. Averin, A. A. Karmanov, et al., Nanomaterials **12**, 1924 (2022). https://doi.org/10.3390/nano12111924
23. S. Agarwal, L. K. Jangir, K. S. Rathore, et al., Appl. Phys. A **125**, 553 (2019). https://doi.org/10.1007/s00339-019-2852-x
24. K. Sabzehei, S. H. Hadavi, M. G. Bajestani, et al., Solid State Sci. **107**, 106362 (2020). https://doi.org/10.1016/j.solidstatesciences.2020.106362
25. J. Wang, Z. Wang, B. Huang, et al., ACS Appl. Mater. Interfaces **4**, 4024 (2012). https://doi.org/10.1021/am300835p
26. P. Singh, V. Mishra, S. Barman, et al., J. Alloys Compd. **889**, 161663 (2021). https://doi.org/10.1016/j.jallcom.2021.161663
27. X. Feng, B. Lv, L. Lu, et al., Appl. Surf. Sci. **562**, 150106 (2021). https://doi.org/10.1016/j.apsusc.2021.150106
28. N. Kamarulzaman, M. F. Kasim, and R. Rusdi, Nanoscale Res. Lett. **10** (2015). https://doi.org/10.1186/s11671-015-1034-9
29. I. A. Pronin, N. D. Yakushova, A. A. Karmanov, et al., Glass Phys. Chem. **44**, 464 (2018). https://doi.org/10.1134/S1087659618050140
30. I. A. Pronin, N. D. Yakushova, I. A. Averin, et al., Inorg. Mater. **57**, 1140 (2021). https://doi.org/10.1134/S0020168521110108
31. Y. Cao, J. Luo, W. Huang, et al., J. Chem. Phys. **152**, 074714 (2020). https://doi.org/10.1063/1.5138372

Translated by D. Churochkin